Phase diagram of a hard-sphere system in a quenched random potential: A numerical study

Chandan Dasgupta*
Centre for Condensed Matter Theory, Department of Physics, Indian Institute of Science, Bangalore 560012, India

Oriol T. Valls†
School of Physics and Astronomy and Minnesota Supercomputer Institute, University of Minnesota, Minneapolis, Minnesota 55455-0149
(Received 8 February 2000)

We report numerical results for the phase diagram in the density-disorder plane of a hard-sphere system in the presence of quenched, random, pinning disorder. Local minima of a discretized version of the Ramakrishnan-Yussouff free energy functional are located numerically and their relative stability is studied as a function of the density and the strength of disorder. Regions in the phase diagram corresponding to liquid, glassy, and nearly crystalline states are mapped out, and the nature of the transitions is determined. The liquid to glass transition changes from first to second order as the strength of the disorder is increased. For weak disorder, the system undergoes a first-order crystallization transition as the density is increased. Beyond a critical value of the disorder strength, this transition is replaced by a continuous glass transition. Our numerical results are compared with those of analytical work on the same system. Implications of our results for the field-temperature phase diagram of type-II superconductors are discussed.

PACS number(s): 64.70.Pf, 64.60.Ak, 64.60.Cn

I. INTRODUCTION

The equilibrium phase diagram of a classical system of interacting particles in a quenched, random, pinning potential is an active and important subject of research [1]. Systems such as vortices in the mixed phase of high-T_c superconductors [2], fluids confined in porous media [3], magnetic bubble arrays [4], and Wigner crystals [5] provide physical realizations of a collection of interacting classical objects in the presence of an external, time-independent, random potential. In the absence of such a potential, systems of this kind are expected to crystallize at low temperatures. Several years ago, Larkin [6] showed that arbitrarily small amounts of random pinning disorder destroy long-range translational order in all dimensions $d<4$. However, recent theoretical studies [7,8] suggest that weak disorder distorts the crystalline state only slightly, leading to a phase with perfect topological order and logarithmic fluctuations of the relevant displacement field. This phase, with quasi-long-range translational order and power-law Bragg peaks in the structure factor, is called a ''Bragg glass'' [8]. The transition point between a Bragg glass and the high-temperature liquid phase is likely to be shifted with increasing disorder, but the transition is believed to remain first order as long as the disorder is weak. A question of obvious interest is how this transition temperature and the nature of the transition depend on the strength of the random potential.

As the strength of the disorder is increased, the Bragg glass phase is expected to undergo a transition to a topologically disordered amorphous phase with only short-range correlations. It is not yet clear whether this phase is thermodynamically distinct from the high-temperature liquid. An interesting possibility is that it is analogous to the glassy phase obtained by supercooling a liquid below the structural glass transition temperature in the absence of external quenched disorder [9]. If this is so, then the phase diagram of such systems would contain three phases: a Bragg glass phase obtained at low temperature and weak disorder, an amorphous (without quasi-long-range translational order) glassy phase at low temperatures and strong disorder, and a weakly inhomogeneous (because of the random potential) liquid phase at high temperatures. The glassy phase would be thermodynamically stable in these systems. This is different from the situation in the absence of external disorder where the crystalline state is the true equilibrium state near the structural glass transition and both the supercooled liquid and the glass are metastable. Thus, the presence of external disorder may lead to the possibility of occurrence of a true, thermodynamically stable, glassy phase.

The phase diagram [2] in the temperature (T)–magnetic field (H) plane of layered, highly anisotropic, type-II superconductors such as $Bi_2Sr_2CaCu_2O_8$ in a magnetic field perpendicular to the layers is a credible candidate to exhibit these three phases. For a wide range of values of H, the flux lines in these materials may be regarded as columns of interacting ''pancake'' vortices [2] residing on the layers, and the properties of the mixed phase may be described in terms of the classical statistical mechanics of these pointlike objects. At low enough fields, a flux-lattice melting transition separates a nearly crystalline state of the flux lines from a disordered ''vortex liquid'' state. The first-order character of this transition has been carefully documented [10]. When H is increased, the transition becomes continuous [10,11], and the nearly crystalline state appears to be replaced by a ''vortex glass'' [12] that has glassy properties such as non-Ohmic current-voltage characteristics [13]. It is generally assumed [12] that the vortex glass phase owes its existence to the presence of pointlike pinning disorder. Observation of Bragg

*Also at the Condensed Matter Theory Unit, Jawaharlal Nehru Center for Advanced Scientific Research, Bangalore 560064, India. Electronic address: cdgupta@physics.iisc.ernet.in

†Electronic address: otvalls@tc.umn.edu

peaks in neutron scattering experiments [14] confirms that the phase at low H and T is a Bragg glass. As the strength of the disorder is increased, either indirectly by increasing H (which is believed to increase [11] the effective strength of the disorder), or directly by increasing the amount of sample defects [15], the Bragg glass phase changes over to the vortex glass. The latter is separated from the liquid by a continuous transition [16]. Thus, this phase diagram suggests that the first-order liquid-to-crystal transition in a three-dimensional system of pointlike objects may be driven by the pinning disorder into a continuous liquid-to-glass transition.

The formation of a glassy phase at strong disorder was recently investigated analytically [17] in a study of the phase diagram of a system of hard spheres in a random pinning potential. This work used a combination of two ''mean-field''-type approaches based on the ''replicated liquid formalism'' [3,18,19]: the replica method [20] was used for treating the effects of quenched disorder, and the hypernetted chain approximation [21] to calculate the equilibrium correlation functions in the liquid in the presence of the pinning potential. These correlation functions were then the input in a replicated density functional [18] of the Ramakrishnan-Yussouff (RY) form [22] from which the location of the freezing transition of the liquid into a nearly crystalline (Bragg glass) phase was obtained. The possibility of a liquid-to-glass transition was investigated using the phenomenological approach of Mézard and Parisi [19]. The resulting [17] phase diagram in the density-disorder plane (the density, rather than the temperature, is the appropriate control parameter for a hard-sphere system) shows three phases: a nearly crystalline Bragg glass, an amorphous glassy phase, and a low-density liquid. It is consistent with the expectation (from earlier work [18] and the Lindemann criterion [23]) that the density at which the Bragg glass to liquid transition occurs should move to higher values as the strength of the disorder is increased. The first-order crystallization transition is replaced by a continuous glass transition as the disorder strength is increased above a threshold value. This phase diagram is, thus, qualitatively similar to that proposed for some layered type-II superconductors if, as noted above, the density is replaced by the temperature T and the disorder strength by the magnetic field H.

Here, we report the results of a numerical investigation of the phase diagram of the same system: a hard-sphere fluid in the presence of a random pinning potential with short-range spatial correlations. We use direct numerical minimization to study the effects of the presence of a random potential on the minima of a discretized version of the RY free-energy functional for the hard-sphere system. In the absence of external disorder, this model free-energy functional exhibits, at sufficiently high densities, a large number of ''glassy'' local minima [24] characterized by inhomogeneous but aperiodic density distributions. A global minimum corresponding to the crystalline solid is also found at high densities if the sample size and the discretization scale are commensurate with the crystal structure. We have carried out extensive numerical investigations of the resulting free-energy landscape [25–28] in the absence of disorder. In this study, we develop similar numerical methods to find the location and structure of the local minima of the same model free energy with the addition of a time-independent, random, one-body potential.

Using these numerical methods we investigate how the uniform liquid, crystalline solid, and glassy minima of the free energy in the absence of the random potential evolve as the strength of this potential is increased. We also examine the dependence of the free energy and the density structure of these minima on the strength of the disorder. In this picture, a transition from one phase to another is signaled by the crossing of the free energies of the corresponding minima of the free energy. By monitoring where these crossings occur as the density and the strength of the disorder are varied, we are able to map out the phase diagram in the density-disorder plane. This phase diagram is qualitatively very similar to the one obtained in the analytic work [17]. For weak disorder we find, in the commensurate case as described earlier where a crystalline minimum exists, a first-order liquid-to-crystal transition that moves to higher density as the disorder is increased. In the metastable ''supercompressed'' regime (i.e., at a density higher than the value at which equilibrium crystallization takes place for the commensurate case), we find in all cases a liquid-to-glass transition. The density at which this transition occurs decreases (very slowly for the largest systems studied, which are incommensurate, and more rapidly for the smaller, commensurate systems) as the disorder is increased. The nature of this glass transition depends on the strength of the disorder: it is first order when the disorder is weak, but it changes to second order beyond a certain critical value of the disorder strength. For the commensurate case, the crystallization line crosses the glass transition at or very near the same critical value of the disorder strength, so that the system at stronger disorder then undergoes a liquid-to-glass transition (instead of the liquid-to-crystal transition found for weak disorder) as the density is increased. The continuous nature of the glass transition in the large disorder regime is in contrast with the first-order transition from the liquid to a crystalline or glassy state (depending on the commensurability) at small values of the disorder strength. Thus, this work supports the prediction that the first-order liquid-to-crystal (Bragg glass) transition should change over to a continuous liquid-to-glass transition as the strength of the pinning disorder is increased beyond a critical value.

The rest of the paper is organized as follows. In Sec. II, we define the model studied here and outline the numerical procedure used. The results obtained for the different transition lines in the density-disorder plane are described in Sec. III. Section IV contains a summary of our main results and a few concluding remarks.

II. METHODS

A. The free-energy functional

As discussed in the Introduction, our starting point is the free energy as a functional of the time-averaged local density $\rho(\mathbf{r})$ at each point $\mathbf{r}$. We write this free energy functional in the form

$$F[\rho]=F_{RY}[\rho]+F_s[\rho], \tag{2.1}$$

where the first term in the right-hand side is the RY free-energy functional [22] for hard spheres in the absence of

disorder, and the second is the contribution arising from the presence of a quenched random potential. Thus, we have

$$\beta F_{RY}[\rho] = \int d\mathbf{r}\{\rho(\mathbf{r})\ln[\rho(\mathbf{r})/\rho_0] - \delta\rho(\mathbf{r})\} - \frac{1}{2}\int d\mathbf{r}\int d\mathbf{r}' C(|\mathbf{r}-\mathbf{r}'|)\,\delta\rho(\mathbf{r})\,\delta\rho(\mathbf{r}'). \tag{2.2}$$

Here, we have defined $\delta\rho(\mathbf{r}) \equiv \rho(\mathbf{r}) - \rho_0$ as the deviation of $\rho(\mathbf{r})$ from ρ_0, the density of the uniform liquid, and taken the zero of the free energy at its uniform liquid value. In Eq. (2.2), $\beta = 1/(k_B T)$, T is the temperature and the function $C(r)$ is the direct pair correlation function [21] of the uniform liquid at density ρ_0, which can be analytically expressed in terms of the usual dimensionless density for hard spheres of diameter σ, $n^* \equiv \rho_0 \sigma^3$, by making use of the Percus-Yevick approximation [21] for hard spheres:

$$C(r) = -\frac{(1+2\eta)^2}{(1-\eta)^4}(1+0.5\eta r^3) + 6\eta\frac{(1+\eta/2)^2}{(1-\eta)^4} r \quad (r \leqslant 1), \tag{2.3a}$$

$$C(r) = 0 \quad (r > 1), \tag{2.3b}$$

where η is the packing fraction, $\eta \equiv (\pi/6)n^*$, and the distance r is in units of σ. This approximation is sufficiently accurate in the density ranges ($n^* \leqslant 1.0$) considered in this paper. We write also

$$\beta F_s[\rho] = \int d\mathbf{r}\,\delta\rho(\mathbf{r})V_s(\mathbf{r}), \tag{2.4}$$

where $V_s(\mathbf{r})$ is an external potential (in dimensionless form) representing the random, quenched disorder. We will assume that V_s has zero mean and short-range Gaussian correlations as detailed below.

In order to carry out numerical work, we discretize our system. We introduce for this purpose a simple cubic computational mesh of size L^3 with periodic boundary conditions. On the sites of this mesh, we define density variables $\rho_i \equiv \rho(\mathbf{r}_i)h^3$, where $\rho(\mathbf{r}_i)$ is the density at site i and h the spacing of the computational mesh. It is known from previous work [24,25] that in the absence of any random potential, this discretized system crystallizes at sufficiently high densities if the quantities h and L are commensurate with a fcc structure with appropriate lattice spacing, whereas no crystalline state exists when the computational mesh is incommensurate with a fcc structure. Both commensurate and incommensurate systems exhibit [24–27] many glassy (inhomogeneous but aperiodic) minima of the free energy at densities higher than the value at which crystallization occurs in commensurate samples.

To model the random potential $V_s(\mathbf{r})$, we introduce random variables $\{V_i\}$ defined at the sites of the computational mesh. These variables are uncorrelated with one another, and distributed according to a Gaussian probability distribution with zero mean and variance s. Thus, s represents the dimensionless strength of the disorder. In terms of these quantities, the dimensionless free energy of our discretized system has the form

$$\beta F = \sum_i \{\rho_i \ln(\rho_i/\rho_\ell) - (\rho_i - \rho_\ell)\} - \frac{1}{2}\sum_i \sum_j C_{ij}(\rho_i - \rho_\ell)(\rho_j - \rho_\ell) + \sum_i V_i(\rho_i - \rho_\ell), \tag{2.5}$$

where the sums are over all the sites of the computational mesh, $\rho_\ell \equiv \rho_0 h^3$, and C_{ij} is the discretized form of the direct pair correlation function $C(r)$ of the uniform liquid.

The thermodynamics of hard spheres in the clean limit is determined by the dimensionless density n^* only. Our rescaling of the potential V_s by β [see Eq. (2.4)] ensures that s is now the only additional relevant variable. Our objective is to study the phase diagram of this system in the (n^*, s) plane. In our mean-field description, different phases are represented by different minima of the free energy. If several local minima of the free energy are simultaneously present, then the minimum with the lowest free energy represents the thermodynamically stable phase and the other local minima correspond to metastable phases. A crossing of the free energies of two different minima signals a first-order phase transition. The point where a minimum becomes locally unstable (i.e., changes from a true minimum to a saddle point or disappears altogether) corresponds to a mean-field spinodal point representing the limit of metastability of the corresponding phase. A merging of the transition point with the spinodal points of the two phases signals a continuous phase transition in this description. Thus, a study of how the minima of the free energy of Eq. (2.5) evolve as n^* and s are changed is sufficient for mapping out the mean-field phase diagram in the (n^*, s) plane.

Locating the minima of the free energy is a difficult numerical problem. The crystalline and glassy minima are highly inhomogeneous with the values of the density variables $\{\rho_i\}$ ranging over more than 12 orders of magnitude. Also, the constraints, $\rho_i \geqslant 0$ for all i, must be satisfied for any physical minimum. For these reasons, standard, numerically efficient minimization methods cannot be readily applied to this problem. We have used a numerical procedure generalized from that originally developed for the clean case [24]. This procedure works by changing the local density variables $\{\rho_i\}$ in a way that ensures that these changes always decrease the free energy. Given an initial configuration of the variables $\{\rho_i\}$, this procedure finds, by constantly moving downhill on the free-energy surface in the multidimensional configuration space spanned by the L^3 variables $\{\rho_i\}$, the local minimum whose basin of attraction contains the initial state. Thus, different local minima of the free energy can be located by using this minimization procedure for different, appropriately chosen, initial configurations. While this procedure is numerically stable and guaranteed to converge to a local minimum, it is not very efficient, often requiring thousands of iterations for convergence. For this reason, our study is restricted to relatively small systems, few realizations of the disorder and coarse discretization scales.

As noted earlier, there are in our system three different kinds of free-energy minima: liquid, crystalline, and glassy. In the clean limit ($s=0$), it is easy to distinguish among them: the liquid minimum has uniform density, the crystalline minimum has a periodic distribution of the density variables, and a glassy minimum exhibits a strongly inhomogeneous nonperiodic density distribution. This symmetry-based distinction among minima of different kinds becomes less clear when the external random potential is turned on: for $s \neq 0$, the density distribution in the liquid phase is not completely homogeneous, and the crystalline state is not strictly periodic.

Therefore we use here a procedure of ''adiabatic continuation'' to distinguish among the liquid, crystalline, and glassy minima in the presence of the disorder. This procedure works as follows: We start with a minimum of a particular kind obtained at $s=0$ for a given value of n^*. There is no difficulty in generating the liquid (and if appropriate the crystalline) configuration for the pure system. Glassy states at $s=0$ are easily obtainable also, in the right density ranges, by the procedures described in Ref. [27]. Indeed, we have used in many cases the same density configurations obtained there that were available as computer files. After thus choosing the initial state, we generate a set of uncorrelated random numbers r_i, $i=1,\ldots,L^3$, distributed according to a Gaussian with unit variance. A ''realization'' of the random potential $\{V_i\}$ is obtained by multiplying these random numbers by the strength parameter s. The initial $s=0$ minimum is then ''followed'' to finite s by increasing s in small steps δs [29]. After each step increase, the minimization routine is run to find the nearest local minimum, using the configuration at the minimum obtained at the previous step as the starting point. During this process, the random variables $\{r_i\}$ are held fixed—only the strength parameter s in increased in steps of δs. By iterating this procedure, minima of different kinds obtained at $s=0$ for a certain n^* are ''followed'' at constant density to the desired value of s. We use the terms ''liquid,'' ''crystalline,'' and ''glassy'' to denote the continued $s \neq 0$ minima obtained from a $s=0$ minimum of the corresponding kind by using this continuation procedure without crossing transition lines. We will show that even at larger s the different kinds of minima have distinguishable structures.

Once a minimum of the desired kind is obtained at a particular point in the (n^*,s) plane, the translational correlations at the minimum can be quantified by the two-point correlation function $g(r)$ of the density variables $\{\rho_i\}$. This function is defined as

$$g(r)=\sum_{i>j} \rho_i \rho_j f_{ij}(r) \Big/ \left[\overline{\rho}^2 \sum_{i>j} f_{ij}(r) \right], \tag{2.6}$$

where the distance r is measured in units of σ, $\overline{\rho} \equiv \Sigma_i \rho_i / L^3$ is the average value of the ρ_i variables at the minimum under consideration, and $f_{ij}(r)=1$ if the separation between mesh points i and j lies between r and $r+\Delta r$ (Δr is a suitably chosen bin size), and $f_{ij}(r)=0$ otherwise. This function represents the spatial correlation of the *time-averaged* local density, and is distinct from the *equal-time*, two-point density correlation function that is often called $g(r)$ in the literature. We also calculate ρ_{max}, the maximum value of the ρ_i variables at the minimum, which gives additional information about the inhomogeneity when contrasted with $\overline{\rho}$ or its rescaled equivalent $\rho_{av} \equiv \overline{\rho}(\sigma/h)^3$ at the minimum.

In addition to examining the transitions by looking at F, $g(r)$, and the density configurations, we also directly check on the stability of the corresponding minima. The stability of a local minimum requires that all the eigenvalues of the Hessian matrix $\mathbf{M}$ whose elements are given by

$$M_{ij} \equiv \frac{\partial^2(\beta F)}{\partial \rho_i \partial \rho_j} = \frac{1}{\rho_i}\delta_{ij} - C_{ij} \tag{2.7}$$

evaluated at the minimum must be positive. This matrix is difficult to handle numerically if the minimum under consideration is strongly inhomogeneous, with some of the ρ_i's very close to zero. In such cases, the $1/\rho_i$ in the first term on the right-hand side of Eq. (2.7) causes numerical difficulties. To avoid this problem, we consider instead the closely related matrix $\mathbf{M}'$ whose elements are given by

$$M'_{ij} \equiv \sqrt{\rho_i} M_{ij} \sqrt{\rho_j} = \delta_{ij} - C_{ij}\sqrt{\rho_i \rho_j}, \tag{2.8}$$

evaluated at the minimum under consideration. It is easy to show that an instability of the minimum corresponds to the vanishing of the smallest eigenvalue λ of this matrix. In our numerical work, we calculate the value of λ in order to check whether the minimum under study becomes unstable as n^* or s is varied.

In our computations we have included the density range from $n^*=0.65$ to $n^*=0.95$, and values of s from zero to about two. These are sufficient to encompass the phenomena we wish to study. We have used three lattice sizes, $L=12,15$, and 25. For the last two we have used an incommensurate ratio $h/\sigma=1/4.6$, whereas for the smallest lattice we have taken the commensurate value $h/\sigma=0.25$.

III. RESULTS

A. General considerations: Phase diagram

Consider first the previously studied [24,27,28] case of the disorder-free system ($s=0$ line). There, only the uniform liquid minimum is present at low densities. As n^* increases, a crystalline minimum appears if the computational mesh is commensurate. When n^* is further increased, a density is reached at which the crystal becomes thermodynamically stable, that is, its free energy becomes lower than that of the liquid state. We will denote this density as n_D^*. Regardless of commensurability, many glassy minima appear as the density is further increased. We denote by n_C^* the density at which the first glassy minimum makes its appearance. Alternatively, one may consider the evolution of the glassy minima as n^* is *decreased* from a large initial value, and define n_C^* as the density at which the last remaining glassy minimum becomes locally unstable and disappears: the free energy of this last remaining glassy minimum crosses that of the liquid at a density n_B^* that is somewhat higher than n_C^*. This density corresponds to a liquid-to-glass transition. In the commensurate case, the density n_C^* is above the crystallization density n_D^*, and the free energy of the crystalline mini-

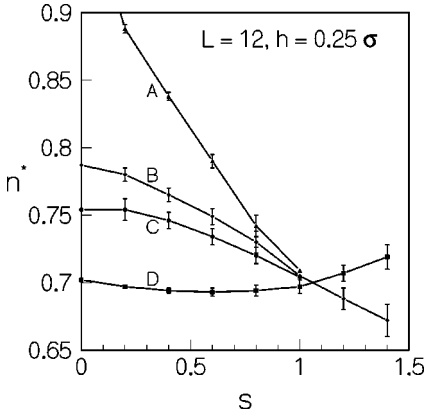

FIG. 1. The overall phase diagram of the hard-sphere system in the density (n^*)-disorder (s) plane, obtained for the $L=12$ commensurate sample, where $n^* \equiv n\sigma^3$ is the dimensionless density and s is the dimensionless strength of the random potential. The meaning of the line labels is explained in the text. The results shown are averages over five realizations of the disorder. The error bars shown are calculated from sample-to-sample variations.

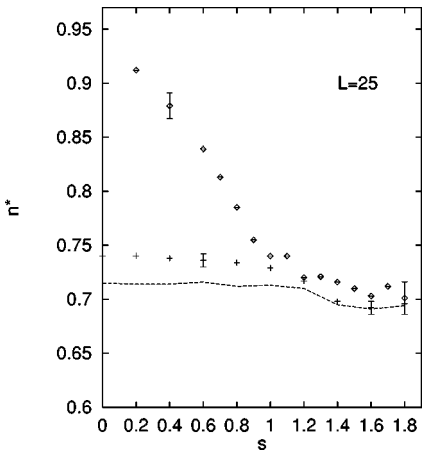

FIG. 2. The overall phase diagram for the incommensurate case at size $L=25$ as explained in the text. The diamonds represent the A line, the crosses the B line, and the dashed line is the C line. Sample error bars have also been included. They reflect sample-to-sample variations for 6–12 (the number increases with s) realizations of the disorder.

mum is lower than that of the glassy minima. Thus, the glass transition in the pure system occurs in a ''supercompressed'' regime where the crystalline state is the thermodynamically stable one.

When we include the effects of the disorder ($s>0$), we find yet another density, n_A^*, at which the liquid minimum becomes locally unstable (i.e., ceases to exist as a local minimum of the free energy). For weak disorder, the value of n_A^* is large (substantially higher than n_B^*) so that the four densities n_A^*, n_B^*, n_C^*, and n_D^* are in decreasing order. Thus, we have four (three in the incommensurate case where the crystalline state is absent) functions $n_X^*(s)$ with $X=A,B,C,D$ representing precisely the four transitions or instabilities defined above. We denote the corresponding lines in the (n^*,s) plane as the A,B,C,D lines. The determination of the location of these lines is one of the main results of our work. These results will be discussed below, but to fix ideas and to make this discussion easier to follow, we show in Fig. 1 these four lines for the $L=12$ commensurate case. There, the general structure of the phase diagram, including the general shape of the four lines $n_X^*(s)$ can be seen. Similarly, we show in Fig. 2 the three lines $n_X^*(s), X=A,B,C$ (from top to bottom) found in the incommensurate, $L=25$ system. The similarities and differences between the commensurate and incommensurate cases are discussed below. The lines in the phase diagram for the incommensurate $L=15$ case are within error bars the same as those shown in Fig. 2, so that the differences between Figs. 1 and 2 must be attributed to different commensurability rather than to different sample size.

There are certain trends that can be easily discerned when one follows a free-energy minimum as s is increased at constant n^*. If one starts from the uniform liquid minimum at $s=0$ and a relatively small value of n^*, the free energy value at the minimum (initially zero according to our convention) decreases steadily with increasing s. The density distribution becomes progressively less uniform, with ρ_{max}, which at $s=0$ equals the average value $\overline{\rho}=\rho_\ell$, rising by more than one order of magnitude as s increases from zero to one. For a deep glassy state at a relatively large value of n^*, the free energy is strongly negative even at $s=0$, and its value decreases further as s increases. The density distribution at such a glassy minimum is considerably more inhomogeneous than that of the liquid minimum continued to the same value of s and it is less sensitive to the value of s: the quenched disorder has less effect on a state that is inhomogeneous and disordered to begin with.

These trends in the behavior of liquid and glassy minima as s is increased from zero are clearly illustrated by examining the pair correlation function $g(r)$, defined in Eq. (2.6), at each minimum. In Fig. 3, we show $g(r)$ computed for the liquid minimum at size $L=25$ and density $n^*=0.66$. The curves shown, in order of increasing value of the peak near $r=1$, correspond to increasing values of $s=0.2,0.6,1.0,1.4,1.8$. There is a clearly visible increase in structure that becomes more evident as the value of s increases beyond

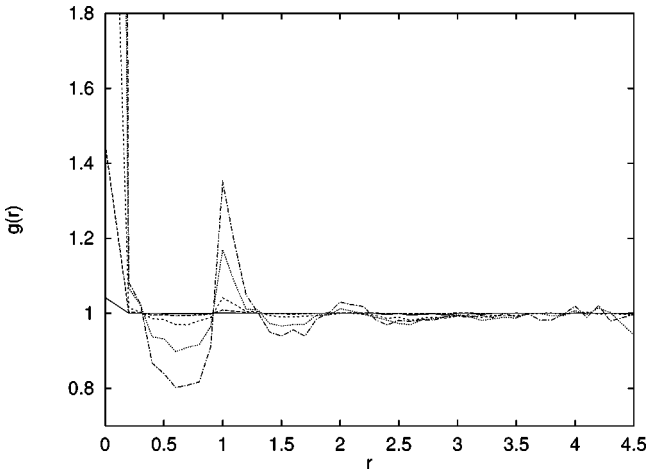

FIG. 3. Liquid phase correlations. The pair correlation function $g(r)$ as defined in Eq. (2.6) plotted as a function of the dimensionless quantity r, defined as the distance in units of σ, for the liquid-like minimum at density $n^*=0.66$. The curves shown, in order of increasing peak height at $r=1$, correspond to $s=0.2,0.6,1.0,1.4,1.8$. The system size is $L=25$.

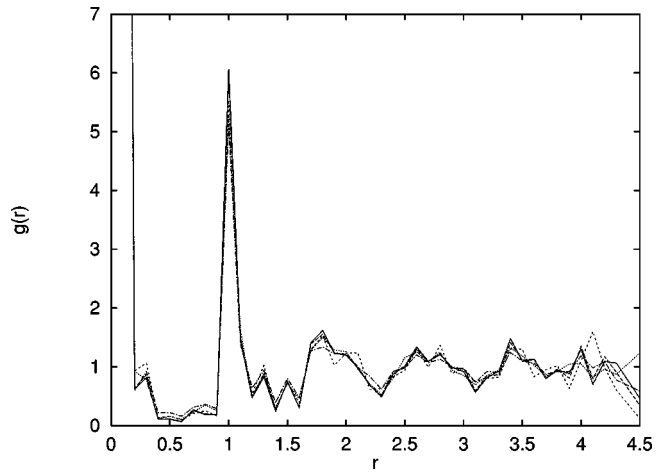

FIG. 4. The pair correlation function $g(r)$ for a glassy minimum. The curves shown correspond to the same values of L and s as in Fig. 3, but for a glassy minimum at $n^*=0.78$ as discussed in the text.

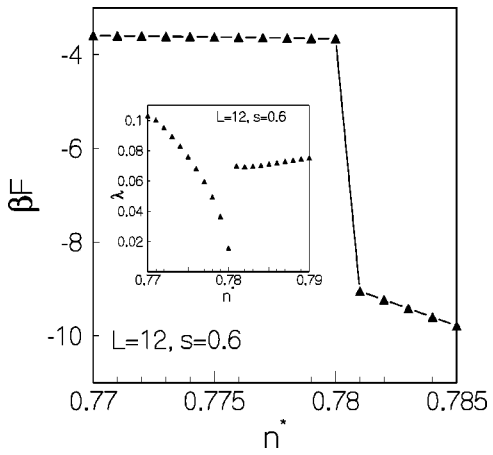

FIG. 5. Discontinuities at the A line. In the main plot, the free energy in dimensionless form for a $L=12$ sample ($s=0.6$) is plotted as a function of the dimensionless density variable n^*. A sharp drop in the free energy is seen as the liquid minimum becomes unstable and the system switches to a glassy minimum. As shown in the inset, this switch is also reflected in the discontinuity in λ, the smallest eigenvalue of the matrix $\mathbf{M}'$ defined in Eq. (2.8).

unity. However, this level of structure is still quantitatively different from that found for glassy minima at relatively high densities. This can be seen by comparing Fig. 3 with Fig. 4 where we plot $g(r)$ for a $L=25$ glassy minimum continued from $s=0$ to $s=1.8$ at $n^*=0.78$. We see that the s dependence of the structure is now much weaker, and the heights of the peaks at $r=0$ and near $r=1$ are much larger than those in Fig. 3. These results can be compared to those found in the replica calculation [17]. To make contact with those results, our $g(r)$ for the liquidlike minimum should be compared with the function $g_0(r)$ of the replica symmetric solution, and our $g(r)$ for a glassy minimum with the function $g_1(r)$ of the replica-symmetry-broken solution. Although, due to differences in the modeling of the random potential and effects of discretization in the present study (some of these effects are discussed in Sec. IV), a detailed, quantitative comparison of our results with those of Ref. [17] is not possible, it is clear that the main features we have discussed are qualitatively similar.

The crystalline minimum obtained for $s=0$ in commensurate systems at sufficiently high densities shows very little change in structure as it is followed to nonzero values of s. Any effects of weak pinning disorder on the crystalline order may be too subtle [6,8] to show up at the system sizes and discretization scales used here.

B. Instability of the liquid minimum

We consider first the A line, that is, the density at which the liquid minimum becomes locally unstable as n^* is increased from a low initial value, keeping s fixed. This transition is detected at any desired value of s in the following way. At a density previously determined to be well below the value of $n_A^*(s)$ (this determination is easily performed by trial and error), one ''follows'' the $s=0$ liquid minimum, as previously explained, to the value of the disorder strength being studied. The density configuration at this minimum is the initial condition. Then, one proceeds to increase n^* by small intervals, thus moving up along a vertical line in the phase diagram. At every value of n^* that is reached, we run our minimization routine (using the configuration at the minimum obtained at the previous step as the starting point) to locate the nearest minimum. The density configuration at the minimum is analyzed and then used as the initial condition to study the next higher density.

In the initial stages of this process, the system remains in the liquidlike minimum, with little change in its properties. However, as n^* reaches the value $n_A^*(s)$, discontinuities are found. These are more prominent for the larger system sizes (Fig. 2) and particularly dramatic for values of s not too large. As the liquid minimum becomes unstable, the system has to find some other nearby minimum (our numerical minimization procedure is designed to converge only to stable local minima of the free energy). Computationally, this is heralded by a very sharp and obvious increase in the number of iterations required by our numerical procedure to find the free-energy minimum nearest to the starting configuration. This new minimum is invariably glassy, as one might expect, since a considerable number of glassy minima are close in configuration space to the liquidlike minimum [27]. The value of the free energy at the minimum that the system has reached drops sharply as the $n_A^*(s)$ value is crossed, because the free energies of glassy minima are considerably lower in the region of the (n^*,s) plane being considered. Also, every measure of structure in the system increases abruptly, since, as discussed above in connection with Figs. 3 and 4, glassy states are much more inhomogeneous than the liquidlike ones in this region of the (n^*,s) plane.

An example of the behavior found is displayed in Figs. 5 and 6. In the main part of Fig. 5, we show the evolution of the free energy as n^* is increased in steps of 0.001, keeping s fixed at 0.6 for a $L=12$ sample. One can clearly see that βF varies little while the system remains in the liquid minimum and jumps abruptly as this minimum becomes unstable near $n_A^*\simeq 0.78$. The behavior for the larger incommensurate samples is quite similar, the main difference being that the drop in βF is much larger, and that the transition occurs, at this value of s, at $n_A^*\simeq 0.84$ for both $L=15$ and $L=25$. The value of n_A^* can readily be found to very high precision and

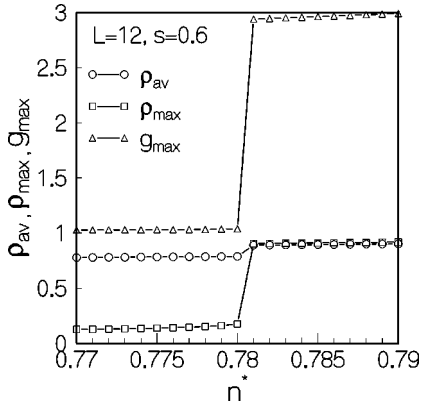

FIG. 6. Example of how the system becomes more structured as the A line is crossed for an $L=12$ sample at $s=0.6$. The height g_{max} of the first finite-r peak in $g(r)$ increases discontinuously, the density nonuniformity represented by ρ_{max} exhibits a large increase, and the average density ρ_{av} shows a small discontinuous increase. In order to be able to use a single vertical scale, we have displayed ρ_{av} rather than $\overline{\rho}$. All plotted quantities are dimensionless (see text).

it varies little as one averages over different realizations of the quenched disorder, for the same s. The error bars shown in Fig. 2 correspond to an average over 6–12 realizations (the larger number at larger s). The results in Fig. 1 are averages over five realizations. In the inset, we show that the smallest eigenvalue λ of the matrix $\mathbf{M}'$ defined in Eq. (2.8) approaches zero as n^* approaches n_A^* from below. This is as would be expected—as noted in Sec. II, the instability of a local minimum is signaled by the vanishing of λ. In Fig. 6, we show three quantities that characterize the nature of the density distribution at a minimum. These are g_{max}, the value of the pair correlation function $g(r)$ at its first finite r maximum (near $r=1$); ρ_{max}, the maximum value of the ρ_i; and the dimensionless average density ρ_{av} defined in Sec. II. All these quantities exhibit discontinuous changes as the system switches minima at $n^*=n_A^*\simeq 0.78$. g_{max} remains close to unity as long as the system stays in the liquid state, and then jumps to a substantially larger value consistent with the increased short-range order present in a glassy minimum. This can also be seen from Figs. 3 and 4. The value of ρ_{max} also increases by a considerable amount, indicating the increased inhomogeneity of a glassy minimum relative to the liquidlike one. The small increase in the value of ρ_{av} reflects that the average density at a glassy minimum is slightly higher than that at the liquidlike minimum.

The behavior discussed above changes as s is increased. The change occurs near $s=1$ for $L=12$, and at somewhat larger s for the other system sizes, as the A,B,C lines come very close to one another. The results obtained in the larger-s regime are described in Sec. III C.

C. Instability of glassy minima and the liquid-to-glass transition

To find the B and C lines, we start with a carefully chosen glassy configuration at a relatively high n^* and fixed s, and then follow this configuration to lower densities by decreasing n^* in small steps ($\delta n^*\simeq 0.001$), keeping the value of s unchanged. This is continued until the minimum becomes unstable and the minimization routine converges to a new minimum which, if the starting minimum is chosen as described below, turns out to be the liquidlike one. The density at which this occurs defines the value of n_C^*. Then, comparing the free energy of the glassy minimum with that of the liquid minimum obtained for the same realization of the disorder, it is easy to determine the value of n_B^*—this is the value of n^* at which the two free energies are equal.

The determination of the appropriate starting glassy minimum is nontrivial. Glassy minima for $s\neq 0$ are obtained by continuation from those of the pure system ($s=0$). One may think that the best choice would be to take the glassy minimum with the lowest free energy at the starting (n^*,s) point. In practice, this is difficult to implement because an exhaustive enumeration of all the glassy minima is computationally very hard. The glassy minimum with the lowest free energy at a particular point in the (n^*,s) plane does not in general continue to have the lowest free energy as the values of n^* and s are changed. Also, in the pure system all the configurations obtained by applying one of the symmetry operations of the computational mesh to the density configuration at a particular glassy minimum also correspond to local minima with exactly the same free energy. For $s\neq 0$, all these symmetry-related minima have to be considered separately because the presence of the random potential destroys the symmetries present in the pure limit.

We have not found a rigorous solution to this problem. Instead, we first carried out an exploratory study of how the locations of the B and C lines in the phase diagram depend on the choice of the initial glassy minimum. The following choices were considered in our initial exploration: (a) one of the low-lying $s=0$ glassy minima, continued to finite s; (b) beginning with the same starting configuration as in (a) and a specific realization of the random variables $\{V_i\}$, minimize the random potential energy [the last term in Eq. (2.5)] with respect to all symmetry operations of the computational mesh. This attempts to find the configuration that minimizes, among all the symmetry related ones, the contribution of the random potential to the free energy but it is not quite rigorous because the minimization is performed using the values of $\{\rho_i\}$ *at the* $s=0$ *minimum*, and (c) the glassy minima to which the system moves when the density is increased above the A line, as discussed in Sec. III B.

The outcome of this study is that the locations of the B and C lines in the (n^*,s) plane are not sensitive to the choice of the glassy minimum as long as it is one of the low-lying minima. (Even when we have deliberately or accidentally chosen a ''wrong,'' non-low-lying minimum, we have found that the system often spontaneously makes a glass-to-glass transition [30] to a low-lying minimum as one decreases n^* above the B line.) The variation of the values of n_B^* and n_C^* for different choices of the glassy minimum is comparable to the uncertainty of these values (shown by the error bars in Figs. 1 and 2) arising from sample-to-sample variations. The results described below were obtained (unless otherwise indicated) from runs in which a low-lying glassy minimum obtained from continuation of one at $s=0$ was taken to be the initial state for the density-lowering run.

For relatively small values of s, the A, B, and C lines are well separated from one another and the signatures of the C instability are very easy to detect: they are similar to the discontinuities shown in Figs. 5 and 6. However, as the value

of s is increased, these three lines begin to approach each other. As shown in Figs. 1 and 2, the separation between lines A and B decreases rather rapidly with increasing s, while the separation between lines B and C decreases more slowly. Finally, near $s=1$, these three lines appear to merge with one another for the $L=12$ system. For $L=25$ (and also for $L=15$), the separation between them does not exceed the combined error bars, but separate B and C transitions can be detected in most (not all) realizations of the disorder, as explained in detail below. At larger s, it becomes increasingly difficult to resolve these three lines. Since lines A and C represent, respectively, the limits of stability of the liquid and glassy minima and line B corresponds to the first-order liquid-to-glass transition, a merging of these three lines suggests that this transition becomes continuous as s is increased beyond a ''tricritical'' value that would be close to unity for the $L=12$ commensurate sample and somewhat larger for the incommensurate samples. Another possibility is that the first-order liquid-to-glass transition disappears beyond a critical point near $s=1$.

To examine the behavior in this region more closely, we have carried out several numerical experiments in which the value of n^* is ''cycled'' through the liquid-to-glass transition, keeping s fixed at values close to unity. In this way, the three lines are detected in the same ''run.'' These numerical experiments are similar to simulations of hysteresis in magnetic phase transitions. We start with the liquid minimum at a low value of n^* (below line C), and increase n^* in small steps, keeping s fixed. The liquid minimum is thus followed to higher densities until it undergoes a rapid change signaling a possible instability. The process of increasing n^* in small increments is continued for a few more steps, and then the local minimum so obtained is followed to lower densities by decreasing n^* in small steps. This is continued until the starting value of n^* is reached. If the liquid-to-glass transition at the chosen value of s is first-order with the three densities n_A^*, n_B^*, and n_C^* separated from one another, then the cycling experiment described above should exhibit clear evidence of hysteresis. This is indeed what we find, for all system sizes and at every run, if the value of s is lower than a certain critical value. A typical example is shown in Fig. 7 which shows the results for a $L=12$ sample at $s=0.8$. The hysteresis in the free energy and g_{max} (shown in the inset) is evident: the liquid minimum becomes unstable at $n_A^* \simeq 0.735$ as n^* is increased from a low initial value, while the glassy minimum found for $n^* > n_A^*$ can be continued all the way down to $n_C^* \simeq 0.720$ before it becomes unstable. The liquid-to-glass transition occurs at $n_B^* \simeq 0.725$ where the two branches of the free energy cross. The same situation occurs for the incommensurate $L=25$ system except that the values of the transition points are $n_A^* \simeq 0.79$, $n_B^* \simeq 0.73$, and $n_C^* \simeq 0.71$ for $s=0.8$. The results at $L=15$ are, within error bars, the same as those for $L=25$ at this value of s.

The behavior in Fig. 7 is to be contrasted with that shown in Fig. 8 that displays the results of the cycling experiment on a $L=12$ sample at $s=1$. The distribution of the random variables $\{r_i\}$ in this sample is the same as that of Fig. 7—only the strength of the disorder is changed. In this figure, there is no evidence of hysteresis in the free energy. The plot of g_{max} shown in the inset exhibits a sharp change near

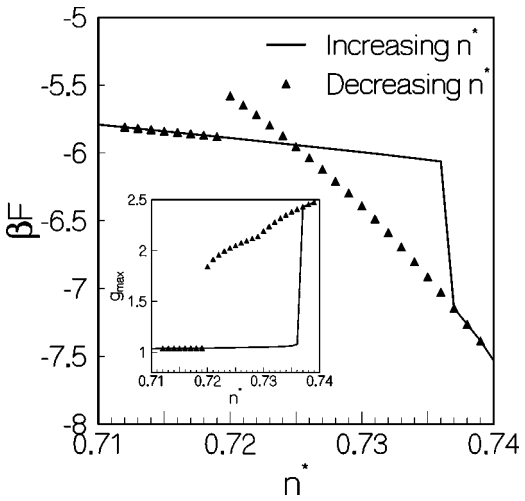

FIG. 7. Hysteresis and discontinuities across the liquid-to-glass transition at small values of s. In the main plot, the dimensionless free energy of the stable minimum is plotted vs density as one cycles across the A, B, and C lines as explained in the text. Hysteresis is clearly observed. In the inset, the quantity g_{max} is shown. The results shown are at $s=0.8$ for a commensurate $L=12$ system, but the same behavior is found in this range of s for incommensurate systems.

$n^*=0.706$ for both increasing-n^* and decreasing-n^* runs, and the results for the two runs are nearly identical. Given the rounding off errors associated with the numerical procedures we use, the small differences between the increasing-n^* and decreasing-n^* values of g_{max} are likely to be insignificant. We, therefore, conclude that at least within the resolution of our numerical procedures, there is no hysteresis at $s=1.0$ for this $L=12$ sample. This implies that the first-order transition found in this sample for $s=0.8$ either becomes a continuous one or disappears as the value of s is increased to 1.0. The sharp change in the value of g_{max} near $n^*=0.706$ suggests that the transition persists as a continuous one. To investigate this further, we have calculated the derivatives of

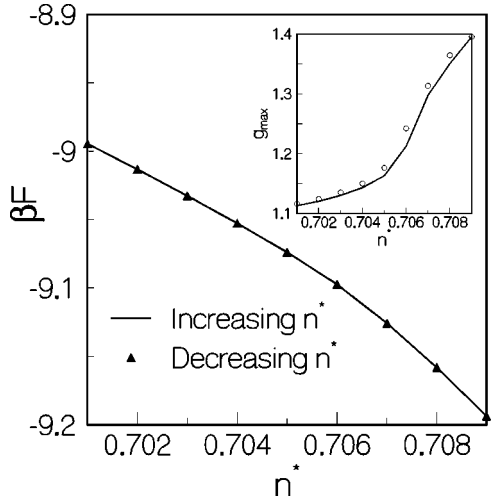

FIG. 8. Cycling across the liquid-to-glass transitions for $s=1$ in a $L=12$ commensurate system. The same quantities are plotted as in Fig. 7, and now no hysteresis is seen. Incommensurate systems exhibit the same behavior at somewhat larger values of s, but not in all runs.

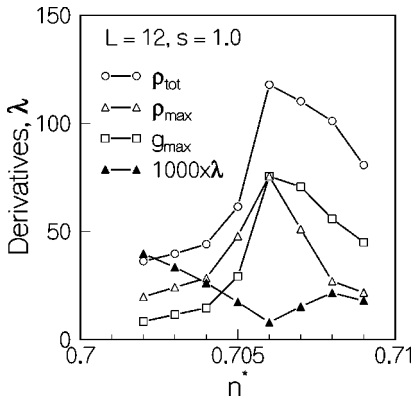

FIG. 9. Derivatives with respect to n^* of the quantities ρ_{tot}, ρ_{max}, and g_{max}, as defined in the text, plotted as functions of n^* across a putatively continuous liquid-glass transition in a $L=12$ sample with $s=1.0$. The three quantities have sharp peaks at $n^*=0.706$. The eigenvalue λ, also defined in the text, shows a pronounced dip at the same point.

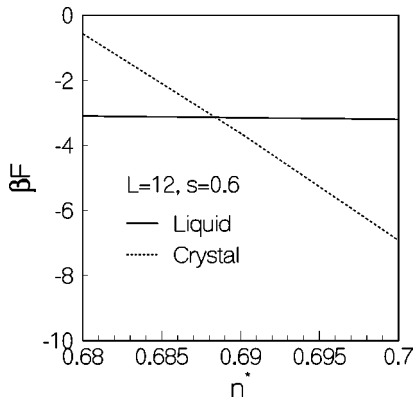

FIG. 10. Free energy crossing at the crystallization transition. The solid and dotted lines represent, respectively, the dimensionless free energies of the crystalline and liquidlike minima of a $L=12$ sample with $s=0.6$. Their crossing point is the density $n_D^*(s)$.

g_{max}, ρ_{max}, and $\rho_{tot}\equiv\Sigma_i\rho_i$ with respect to n^* in the region where these quantities change rapidly. We have also examined the behavior of λ as a function of n^* in this region. Results for these quantities are shown in Fig. 9 for the same sample as that of Fig. 8. All the derivatives exhibit sharp peaks at $n^*=0.706$, and the value of λ goes through a minimum that is very close to zero at the same point. These results strongly suggest the occurrence of a continuous phase transition at $n^*=0.706$. However, due to the limited resolution of our numerical calculations and the smallness of sample size, we cannot rule out the possibility that the observed behavior reflects a sharp crossover rather than a true phase transition. Similar results are found for larger values of *s*. The continuation of the ''transition line'' beyond the point where the lines *A*, *B*, and *C* come together is determined by locating the value of n^* at which the eigenvalue λ reaches a minimum. The value of *s* at which the *A*, *B*, and *C* lines merge and the hysteresis in the cycling experiment disappears is found to be weakly dependent on the realization of the disorder—it varies between 1.0 and 1.2 for the five different $L=12$ samples studied.

For the incommensurate samples, the situation is somewhat more ambiguous. For $L=25$, the same cycling procedure shows that the transition is clearly hysteretic for all runs with $s\leqslant 1.1$. For larger values of *s*, an increasingly larger percentage of the runs is nonhysteretic (i.e., the results for βF look like those in Fig. 8), while the other runs display a behavior similar to that in Fig. 7 but with much smaller discontinuities. As *s* is increased beyond $s=1.8$, it becomes, in most of the ''runs,'' impossible to distinguish the discontinuities, if any, from computer noise. Thus, it is possible in this case to plot separate *A*, *B*, and *C* lines all the way up to $s=1.8$. This accounts for the obvious difference in this respect between Figs. 1 and 2. The results for $L=15$ are quite consistent with those for $L=25$, but the smaller system size makes all interpretations more difficult. Thus, it is more difficult to identify the precise position of any well-defined tricritical point (or a critical point) from the results for the incommensurate samples. One might alternatively say that these incommensurate results are indicative of a crossover. It is not possible to completely rule out that the behavior is different for the commensurate and incommensurate samples, or that the poorer resolution of the smaller samples masks discontinuous behavior in some of the larger *s* runs.

D. Crystallization

To study how the crystallization density n_D^* changes as *s* is increased from zero, we start with the crystalline minimum obtained for a commensurate sample at $s=0$ and a large value of n^*. We then find the symmetry related configuration that minimizes the random potential energy for a particular realization of the disorder and continue this configuration to the desired value of *s*. This configuration is then continued to smaller values of n^* by decreasing n^* in small steps. The crystalline minimum turns out to be quite robust under changes of the density and the strength of the disorder—the minimization routine converges rather quickly to the new minimum as the value of n^* or *s* is changed by a small amount. While decreasing the value of n^*, we keep track of the free energy of the crystalline minimum and find the value of n^* at which this free energy crosses that of the liquid minimum for the same realization of the disorder. For relatively small values of *s*, the crossing point determines the value of n_D^* for the chosen value of *s*. Typical results for the crossing of these two free energies are shown in Fig. 10. Our results for line *D*, averaged over five realizations of the disorder, are shown in Fig. 1. The crystallization transition is strongly first order for all values of *s*. In the small *s* regime, the crystalline minimum has the lowest free energy for all densities above line *D*. Therefore, the lines *A*, *B*, and *C* do not have any equilibrium thermodynamic significance in this regime for a commensurate system: the liquid-to-glass transition at line *B* can be observed only if the crystallization transition at line *D* is avoided, e.g., by rapid compression.

As shown in Fig. 1, the crystallization line crosses the liquid-to-glass transition line at a point that is very close to that where the lines *A*, *B*, and *C* seem to come together. Beyond this point, line *D* is determined by the crossing of the free energies of glassy and crystalline minima. The procedure is quite analogous to that shown in Fig. 10. This line, therefore, represents a first-order transition between crystalline and glassy states in this regime. The phase diagram of Fig. 1 implies that the system undergoes a first-order liquid-

to-crystal transition for small values of s as the density is increased from a low initial value. However, as the value of s is increased above a critical value (which is close to unity for the $L=12$ system), the transition as n^* is increased becomes a continuous liquid-to-glass transition (or perhaps a sharp crossover). The glassy state then undergoes a first-order transition to the crystalline state as the density is increased further. The observed curvature of line D for large s also implies that the system would undergo a first-order crystal-to-glass transition as the strength of the disorder is increased at constant density.

IV. SUMMARY AND DISCUSSION

We have mapped out the mean-field phase diagram of a hard sphere system in the presence of a quenched random potential by numerically studying the evolution of the minima of a model free energy as a function of the density n^* and the strength s of the disorder. The phase diagram in the (n^*,s) plane exhibits liquid, glassy, and crystalline (for commensurate samples) phases. The standard first-order crystallization transition that occurs at $s=0$ upon increasing n^* retains its character at small s as a first-order transition from a weakly inhomogeneous liquid phase to a nearly crystalline state. We also find for all samples a liquid-to-glass transition in the metastable, ''supercompressed'' regime. This transition is first order for small s, but within the resolution of our results, it appears to become continuous as s is increased beyond a critical value, which is larger for incommensurate samples. The crystallization line crosses the glass transition line near the point where the glass transition becomes continuous. Thus, the first-order crystallization transition found for small s as the density is increased from a small initial value is replaced, at sufficiently large s, by a continuous liquid-to-glass transition. The phase diagram also shows a first-order crystal-to-glass transition as s is increased at constant n^*.

The qualitative features of our phase diagram (i.e., its topology, the shapes of the transition and instability lines, and the nature of the transitions) are all identical to those found in the analytic study [17] of the same system [31]. Two of our most important results, the change in the nature of the liquid-to-glass transition beyond a certain value of s and the crossing of the crystallization and glass transition lines above this critical value, were also found in the analytic calculation. This similarity between the results of two studies using extremely different methodologies strongly suggests that the qualitative features of our phase diagram are correct, at least at the mean-field level. The quantitative differences that exist between the numerical and replica results, i.e., that all the transition and instability lines in our phase diagrams lie at substantially lower densities than those obtained in the analytic study, have the same origin as the discrepancy between our $s=0$ results and those of molecular dynamics [32] of the pure hard-sphere system. As noted before [25,28], these differences result from the discretization of the free-energy functional. The use of a simple cubic mesh of spacing $h\sim 0.2\sigma$ in the discretization procedure increases the relative stability of inhomogeneous local minima of the free energy and thus leads to substantially lower values for the densities at which crystallization and the glass transition occur. On the other hand, the quantitative differences between our results in Fig. 1 and those in Fig. 2 appear to arise chiefly from the incommensurability of the latter sample, rather than from the slight difference in the values of h, or even from that in the values of L: we have found negligible sample-size effects in comparing the $L=15$ results to those at $L=25$ at the same value of h. The effects of discretization would presumably disappear for h much smaller than the width of the approximately Gaussian density distributions near the points where the particles are localized at an inhomogeneous minimum of the continuum free-energy functional. Unfortunately, a numerical calculation with such small values ($\sim 0.01\sigma$) of h would require dealing with a very large number (of the order of 10^6) of variables $\{\rho_i\}$. This appears to be computationally difficult, as mentioned in Sec. II.

Possible effects of fluctuations are not included in our mean-field phase diagram. The first-order crystallization transition should not be strongly affected by fluctuations. The situation is more complex for the glass transition because there are a large number of glassy local minima. When fluctuations are included, the system might visit a large number of different glassy minima during its evolution over long times, and thus behave like a liquid in that the particles would no longer be localized in space and the time-averaged local density would be only weakly inhomogeneous. A true thermodynamic glass transition would occur only if the characteristic time scale for transitions between glassy minima diverges in the thermodynamic limit. Whether this happens in the pure system is still a highly controversial issue. Further investigations of this question for systems of particles in the presence of quenched disorder would be very worthwhile. The presence of multiple low-lying glassy minima of the free energy is expected to lead to slow relaxation even if no thermodynamic glass transition is present. Therefore, signatures of the mean-field glass transition found in our study should show up in the dynamics of the system even if no thermodynamic glass transition occurs when fluctuations are taken into consideration.

Our density-disorder phase diagram exhibits qualitative similarities to the field-temperature phase diagram of some high-T_c superconductors in the presence of random point pinning. For a system of vortices in the mixed phase of type-II superconductors, the temperature T plays the role of the density n^* of the hard sphere system—increasing T is analogous to decreasing n^*. As pointed out in the Introduction, increasing the magnetic field H is believed [11] to increase the effective strength of the pinning disorder. Using these analogies, one can translate, in a very crude and qualitative sense, our phase diagram in the (n^*,s) plane to a phase diagram for superconductors in the (T,H) plane. Then, our result that the crystallization transition at weak disorder is replaced by a continuous glass transition as s is increased translates into the statement that for superconductors, the first-order liquid to Bragg glass transition at low fields should change over to a continuous glass transition as H is increased. As noted in the Introduction, this is the behavior found in experiments on a family of high-T_c superconductors. The phase diagram of these superconductors also exhibits a Bragg glass to amorphous solid transition as H is increased at low T. This is analogous to the crystal-to-glass transition found in our phase diagram as s is increased at

constant density. Further evidence in support of this analogy is provided by a recent numerical study [34] that suggests that the high-field, low-temperature phase of high-T_c superconductors (the so-called vortex glass phase) is very similar to a structural glass. In view of these similarities, an extension of our calculation to a system of pancake vortices in layered superconductors with random point pinning, using the appropriate form of the free energy, would be of obvious interest.

We are not aware of any experimentally studied system that provides a direct and precise physical realization of the model studied here. Colloidal suspensions in the presence of a time-independent, spatially random external potential (produced, for example, by suitably configured laser fields [33]) would probably provide a close approximation to our model. Since simple liquids with short-range pair potentials that are strongly repulsive at short distances behave in many ways like a hard-sphere liquid, our calculation is expected to apply, at least qualitatively, to such systems also.

ACKNOWLEDGMENTS

We are grateful to F. Thalmann, G. I. Menon, A. K. Sood, S. Bhattacharya, G. F. Mazenko, and T. Witten for helpful discussions or comments, and to S. Ramasesha for help in the computations.

[1] For a review, see T. Giamarchi and P. Le Doussal, in *Spin Glasses and Random Fields*, edited by A. P. Young (World Scientific, Singapore, 1998).
[2] G. Blatter *et al.*, Rev. Mod. Phys. **66**, 1125 (1994).
[3] E. Lomba, J. A. Given, G. Stell, J. J. Weis, and D. Levesque, Phys. Rev. E **48**, 233 (1993).
[4] R. Seshadri and R. M. Westervelt, Phys. Rev. B **46**, 5142 (1992); **46**, 5250 (1992).
[5] E. Y. Andrei, G. Deville, D. C. Glattli, F. I. B. Williams, E. Paris, and B. Etienne, Phys. Rev. Lett. **60**, 2765 (1988).
[6] A. I. Larkin, Zh. Éksp. Teor. Fiz. **58**, 1466 (1970) [Sov. Phys. JETP **31**, 784 (1970)]; A. I. Larkin and Y. N. Ovchinnikov, J. Low Temp. Phys. **34**, 409 (1979).
[7] T. Nattermann, Phys. Rev. Lett. **64**, 2454 (1990).
[8] T. Giamarchi and P. Le Doussal, Phys. Rev. Lett. **72**, 1530 (1994); Phys. Rev. B **52**, 1242 (1995).
[9] In spite of extensive experimental and theoretical investigation over several decades, the question of whether a true thermodynamic glass transition occurs in supercooled liquids in the absence of disorder remains controversial. In the absence of a clear answer to this question, one may operationally define a ''glass transition'' to occur at the temperature below which the characteristic relaxation time in the liquid exceeds a given value τ_c.
[10] E. Zeldov *et al.*, Nature (London) **375**, 373 (1995).
[11] H. Safar, P. L. Gammel, D. A. Huse, D. J. Bishop, W. C. Lee, J. Giapintzakis, and D. M. Ginsberg, Phys. Rev. Lett. **70**, 3800 (1993).
[12] D. S. Fisher, M. P. A. Fisher, and D. A. Huse, Phys. Rev. B **43**, 130 (1990).
[13] R. H. Koch, V. Foglietti, W. J. Gallagher, G. Koren, A. Gupta, and M. P. A. Fisher, Phys. Rev. Lett. **63**, 1511 (1989).
[14] R. Cubitt *et al.*, Nature (London) **365**, 407 (1993).
[15] B. Khaykovich, M. Konczykowski, E. Zeldov, R. A. Doyle, D. Majer, P. H. Kes, and T. W. Li, Phys. Rev. B **56**, R517 (1997).
[16] The question of whether a true thermodynamic glass phase exists in superconductors with random point pinning is controversial; see, e.g., H. S. Bokil and A. P. Young, Phys. Rev. Lett. **74**, 3021 (1995).
[17] F. Thalmann, C. Dasgupta, and D. Feinberg, Europhys. Lett. **50**, 54 (2000).
[18] G. I. Menon and C. Dasgupta, Phys. Rev. Lett. **73**, 1023 (1994).
[19] M. Mézard and G. Parisi, J. Phys. A **29**, 6515 (1996).
[20] M. Mézard, G. Parisi, and M. A. Virasoro, *Spin Glass Theory and Beyond* (World Scientific, Singapore, 1987).
[21] J. P. Hansen and I. R. McDonald, *Theory of Simple Liquids* (Academic, London, 1986).
[22] T. V. Ramakrishnan and M. Yussouff, Phys. Rev. B **19**, 2775 (1979).
[23] D. Ertaş and D. R. Nelson, Physica C **271**, 79 (1996).
[24] C. Dasgupta, Europhys. Lett. **20**, 131 (1992).
[25] C. Dasgupta and O. T. Valls, Phys. Rev. E **53**, 2603 (1996).
[26] C. Dasgupta and O. T. Valls, Phys. Rev. E **58**, 801 (1998).
[27] C. Dasgupta and O. T. Valls, Phys. Rev. E **59**, 3123 (1999).
[28] C. Dasgupta and O. T. Valls, in *Complex Behavior of Glassy Systems*, edited by M Rubí and C. Pérez-Vicente (Springer, Berlin, 1997).
[29] For the case of the liquid minimum, it is not in fact necessary to make the step δs very small. One gets just the same configuration by directly increasing s from zero to the desired value, basically dropping the system into the right spot in the (n^*,s) plane. To follow the glassy minima, however, more care must be taken. The configurations obtained are independent of δs if this quantity is below 0.05.
[30] We do not attach any significance to the density at which this glass-to-glass transition occurs, and continue to decrease the density until the new glassy minimum becomes unstable and the system converges to the liquid minimum.
[31] Our line *A* should be identified with the line (labeled IN in Fig. 1a of Ref. [17]) at which the replica symmetric solution becomes unstable, line *B* with the line labeled TGT in Fig. 1a of Ref. [17], and line *C* with the ''dynamical transition'' line of Ref. [17] (labeled DT in Fig. 1a there), which corresponds to the first appearance of the replica-symmetry-broken solution. The crystallization line has the same meaning in both calculations.
[32] L. V. Woodcock, Ann. (N.Y.) Acad. Sci. **371**, 274 (1981).
[33] Q.-H. Wei *et al.*, Phys. Rev. Lett. **81**, 2606 (1998).
[34] C. Reichhardt, A. van Otterlo, and G. T. Zimanyi, Phys. Rev. Lett. **84**, 1994 (2000).